

From sea to summit: Investigating the explicit role of SST increase for regional and high-altitude climates in New Zealand

E. Kropač¹, T. Mölg¹, and N. J. Cullen²

¹Climate System Research Group, Institute of Geography, Friedrich-Alexander-Universität Erlangen-Nürnberg (FAU), Erlangen, Germany.

²School of Geography, University of Otago, Dunedin, New Zealand.

Corresponding author: Elena Kropač (elena.kropac@fau.de)

Key Points:

- The explicit effect of ocean warming around New Zealand has impacted the region's hydrothermal climate, winds and moisture transport
- Mesoscale changes include modifications in flow regime, precipitation patterns, foehn effects, and vertical meteorological gradients
- Shifts in high-elevation climate conditions suggest that ocean warming can strongly impact mountain climates and glaciers

Abstract

The oceans around New Zealand are regional warming hotspots where sea surface temperature (SST) is rising much faster than the global average. This has profound ecological, socio-economic and climatic implications, particularly for the Southern Alps, which are highly sensitive to variations in climate. This study uses a sensitivity experiment with a regional atmospheric model to investigate how ocean warming over the past decade (2010–2020) has influenced New Zealand’s climate at different spatial scales, with particular attention to the high-elevation zones of the Southern Alps. The approach addresses the effects of an isolated SST increase, explicitly excluding broader systemic changes associated with global warming.

Results suggest that rising SSTs have driven widespread increases in near-surface air temperature and humidity, particularly in autumn and summer, causing weakened westerlies and altered moisture transport pathways. These larger-scale circulation changes have modified the mesoscale flow regime near the Southern Alps, reshaping precipitation patterns and reducing foehn effects in the eastern lowlands. Crucially, the impacts of the SST increase extend into the alpine environment, where surface warming is amplified and (especially wintertime) snowfall is reduced. Consequently, high-elevation climate regimes have shifted towards warmer and more humid conditions, contributing to greater rainfall dominance and potentially accelerated glacial melt.

This study provides a process-based understanding of the influence of SST changes on both regional and high-altitude climate in New Zealand. The findings emphasize the potential for continued ocean warming to exacerbate high-elevation climate shifts and glacier retreat, with substantial implications for regional hydrology, ecosystems, and human activities.

Plain Language Summary

The oceans around New Zealand are warming much faster than the global average, which impacts the region’s climate. Mountain regions like the Southern Alps are particularly sensitive to variations in climate, as even small shifts in temperature and precipitation can have major impacts on glaciers, ecosystems, and water availability. Determining to what extent ocean warming contributes to these local changes is difficult, as it occurs alongside many other global climate changes.

This study isolates the effects of ocean warming by using an atmospheric model to simulate New Zealand’s climate for 2010–2020 under different sea surface temperature (SST) conditions – one with realistic, observed SSTs and one with modified, colder SSTs reflecting the 1981–2010 average. Comparing the two simulations reveals how rising ocean temperatures alone have influenced the country’s climate over the past decade.

The results show that ocean warming has made New Zealand’s atmosphere warmer and more humid, especially in autumn and summer. This has altered wind patterns and atmospheric moisture transport, leading to changes in precipitation across the South Island. In the high elevations of the Southern Alps, many effects are amplified, with a stronger increase in air temperature, less snowfall and a greater dominance of rainfall.

1 Introduction

Oceans are warming globally by ~ 0.1 °C per decade (1981–2018) due to anthropogenic climate change (Bulgin et al., 2020). This warming trend is particularly pronounced in certain regions, which have been referred to as oceanic or marine "hotspots" (Hobday & Pecl, 2014). One such area is the region around New Zealand – particularly the southwestern Tasman Sea and the southwest Pacific Ocean – where sea surface temperatures (SSTs) have increased nearly four times the global average over the past decades (Oliver et al., 2017; Sutton & Bowen, 2019).

This disproportionate warming has far-reaching ecological, socio-economic and climatic implications. Warmer ocean waters induce heat stress on temperature-sensitive species and promote the spread of invasive taxa. Resulting shifts in species distributions cause disruption to ecosystems and changes to food webs and fish stocks (Keegan et al., 2022; Law et al., 2018). These ecological changes have direct economic consequences, particularly for fisheries and aquaculture, which are vital to New Zealand's economy. Elevated ocean temperatures also fuel more frequent and intense marine heatwaves (Oliver, 2019), that can have more immediate and severe effects, including mass mortality events (e.g., Bell et al., 2024; Thomsen et al., 2019).

Due to the small land mass and the large area of surrounding ocean, New Zealand's terrestrial climate is largely influenced by the surrounding ocean temperatures (Sutton & Bowen, 2019). The South Island of New Zealand is located within the Southern Hemisphere midlatitude storm track, which is perpendicularly intersected by the Southern Alps, a mountain range extending along the west coast of the South Island with several peaks exceeding 3000 m above sea level (Figure 1). The Southern Alps act as a natural barrier to the prevailing westerly flow, thereby modifying the synoptic-scale circulation and creating a pronounced rain shadow effect, with high amounts of precipitation on the west coast of the island and in the mountains (3000 to over 12000 mm a⁻¹) and dry conditions in the east (< 1000 mm a⁻¹) (Griffiths & McSaveney, 1983). The glaciers in the Southern Alps, sustained by substantial snow input from the westerlies, are highly sensitive to variations in both precipitation and, particularly, air temperature (Anderson & Mackintosh, 2006). These factors depend on the characteristics of the transported air masses, which, in turn, are strongly influenced by their predominantly maritime source regions – most notably the Tasman Sea, located directly upstream of the Southern Alps (Lorrey et al., 2022; Purdie et al., 2011). Accordingly, variations in SST around New Zealand have been statistically linked to changes in glacier mass balance, ice volume, seasonal snow, and snowline altitudes in the high-elevation regions of the Southern Alps (Clare et al., 2002; Cullen et al., 2019; Fitzharris et al., 2007, Lorrey et al., 2022; Mackintosh et al., 2017), with especially strong impacts observed during marine or coupled ocean-atmosphere heatwave events (Salinger, Fitzharris, et al., 2019; Salinger, Renwick, et al., 2019; Salinger et al., 2023). Similar statistical links were found for other regions such as Peru (Vuille et al., 2008) or the United States (Christian et al., 2016).

Although widely recognized, the statistical relationship between SST and New Zealand's high-mountain climate, snow and glaciers has not yet been investigated from a process perspective, leaving the physical mechanisms that transmit large-scale SST signals to local

climate anomalies and glacier mass changes ambiguous. However, understanding these physical linkages is crucial, as high-mountain environments are particularly sensitive and vulnerable to changes in climate and play an important role in regional hydrology, ecosystems and tourism (Steiger et al., 2024).

Sensitivity experiments with limited area models (LAMs) are a common tool to investigate the effect of changes in larger-scale surface conditions on regional climate, as shown for the deforestation of the Amazon rainforest (Sierra et al., 2022) or the reduction in Arctic Sea ice (Porter et al., 2012). Several studies have investigated the impact of SST variations on meteorological phenomena such as (extra-)tropical cyclones (Lavender et al., 2018; Miglietta et al., 2011), monsoon rainfall (Sijikumar & Rajeev, 2012), heavy snowfall events (Jung et al., 2012), as well as on coastal air temperature (Takahashi et al., 2015) or the surface mass balance of the Greenland and Antarctic Ice Sheets (Kittel et al., 2018; Noël et al., 2014). A few studies have also investigated the impacts of land-use or SST changes on high-mountain regions and glaciers (Collier et al., 2019; Mölg et al., 2012), but there has been no comparable work in New Zealand.

In this study, we use regional atmospheric modelling and sensitivity experiments with the limited-area Weather Research and Forecasting (WRF) model to investigate the explicit role of SST in influencing atmospheric dynamics and climate variability across the South Island and in the high-elevation regions of the Southern Alps. In particular, we aim to identify how the regional and high-mountain climate have responded to ocean warming around New Zealand over the past decade (2010–2020). Our hypothesis is that the effects of SST variations are not confined to the lowland regions but extend to the high alpine environment, with significant climatic changes detectable in these areas. The study seeks to deepen the understanding of how oceanic changes affect complex local mountain climates, providing insights that could inform climate impact assessments in similar regions worldwide.

2 Data and methods

We utilized the Advanced Research version of the Weather Research and Forecasting (WRF) model v.4.2.2 (Skamarock et al., 2019) to conduct high-resolution atmospheric simulations for the New Zealand region. WRF is a state-of-the-art numerical weather prediction system widely used for both operational forecasting and atmospheric research. It has proven highly valuable in analyzing meteorological processes across different regions, applications, and scales (Powers et al., 2017). The study is based on two WRF simulations, a reference run (REF) and a sensitivity run (SENS), which cover the period from 2010 to 2020 and use the same model setup, except for two modifications in the sensitivity run that are described further below.

The REF run was taken from a previously obtained, 16-year (2005–2020) WRF dataset for New Zealand (Kropač et al., 2023), which has been presented and thoroughly evaluated in Kropač et al. (2024). The model configuration employed two one-way nested domains centred over the Southern Alps (Figure 1), comprising one outer domain (D1) with a horizontal grid spacing of 10 km and one inner domain (D2) at 2 km, both with 60 model levels in the vertical. The simulation was initialized and laterally driven by European Centre for Medium-Range Weather Forecasts (ECMWF) ERA5 reanalysis data (Hersbach et al., 2020) at 31 km spatial

resolution, including the recent warming trend in SSTs. To gently constrain the evolving large-scale meteorological conditions (wind, potential temperature, and water vapor mixing ratio) towards the input fields, analysis nudging (Stauffer & Seaman, 1994) was applied in D1, while the model was allowed to freely evolve in D2. Convective processes were calculated by a cumulus parameterisation in D1 and explicitly resolved in D2. The output frequency was daily (D1) and 3-hourly (D2), respectively. For more detailed information on the model setup and skill of the dataset, refer to Kropač et al. (2024).

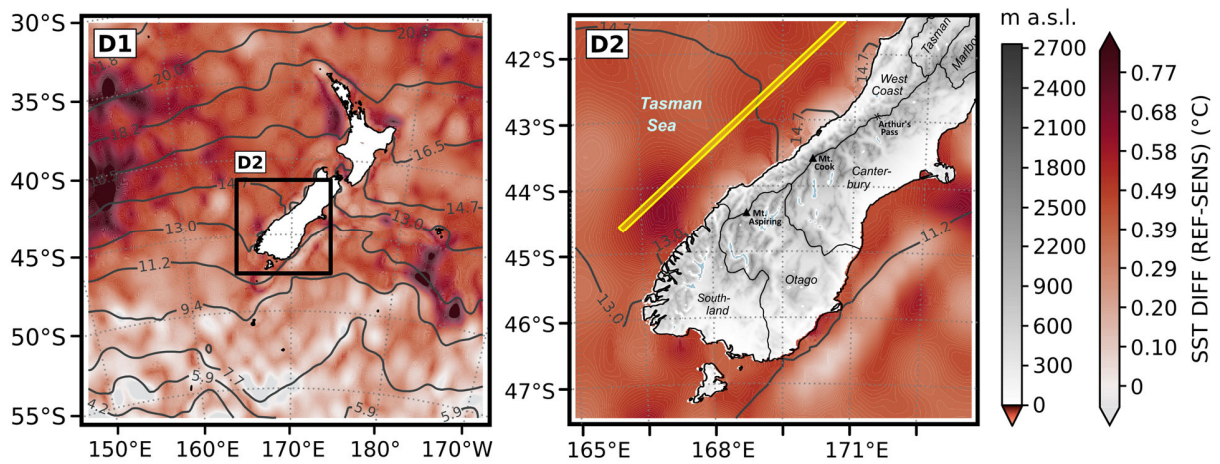


Figure 1. Domain configuration of the WRF model (**left**) and topography in D2 (**right**) with the annual mean SST difference between REF (ocean warming) and SENS (restricted ocean warming) in both domains in 2010–2020. The grey contour lines represent the average SST in 1981–2010 as an absolute reference. The yellow box shows the region used for determining the presumable flow regime of air masses approaching the Southern Alps (1187 grid points; Sect. 3.2.1).

The decadal period from 2010 to 2020 was defined as the study period for the sensitivity experiment, representing a compromise between computational feasibility and climatological relevance. Since 2010, annual mean SST in the New Zealand region (D1 in Figure 1) has consistently exceeded the variance range of the 1981–2010 climate normal period, indicating a considerably warmer background state of upper ocean waters around New Zealand. Additionally, during this period, several climate modes that are relevant for the New Zealand region, such as the El Niño Southern Oscillation (ENSO), the Southern Annular Mode (SAM), the Interdecadal Pacific Oscillation (IPO) and the Pacific Decadal Oscillation (PDO), have exhibited distinct phases, ensuring the incorporation of internal climate variability.

The sensitivity run (SENS) was obtained as a new, 11-year (2010–2020) WRF simulation, utilizing the same model version, configuration and computational setup as the REF run, except for two changes concerning the SST field (1) and the nudging strategy (2):

- (1) The SST field in the ERA5 input data was fixed to the (daily-varying) mean climatological SST from 1981–2010, thus artificially suppressing ocean warming. Consequently, when compared to the climatological baseline, the (unchanged) SST field in the REF simulation exhibits a significant mean increase of 0.37 °C across D1 over the study period (2010–2020) (Figure 1; Table 1). This warming trend is evident across most of the ocean surrounding New Zealand, particularly in the Tasman Sea and the southwest Pacific Ocean southeast of New Zealand. Only the Southern Ocean south of 50° S shows a slight cooling signal, especially in summer (DJF). The most pronounced and widespread SST increase occurs in autumn (MAM), with an average change of +0.49 °C in D1 and +0.61 °C in D2 (Table 1; Figure S1). Mean SST increases in summer and winter (JJA) are lower due to more localized warming, but higher maximum increases are reached (+1.27 °C and +1.44 °C) over the Tasman Sea and the south-west Pacific Ocean, respectively. The smallest SST change occurs in spring (SON) (Table 1; Figure S1). Consistent with this, long-term point measurements since 1967 from both the Hauraki Gulf on the North Island and Portobello on the South Island of New Zealand showed significant warming trends in autumn and winter (Shears & Bowen, 2017; Shears et al., 2024), accompanied by an increase of marine heatwave trends in these seasons (Cook et al., 2022). Similarly, Montie et al. (2024) found that most of the increasing seasonal marine heatwave trends around New Zealand in 1982–2021 were significant in autumn and winter.

Table 1. Minimum, average and maximum change in the annual and seasonal SST field of the outermost (D1) and innermost (D2) WRF domains in the reference run (REF) compared to the sensitivity run (SENS).

		MIN	MEAN	MAX
D1	ANN	-0.21	0.37	0.97
	DJF	-0.47	0.36	1.27
	MAM	-0.24	0.49	1.17
	JJA	-0.34	0.35	1.44
	SON	-0.33	0.28	0.98
D2	ANN	0	0.41	0.66
	DJF	-0.09	0.41	0.80
	MAM	0.21	0.61	0.82
	JJA	-0.22	0.36	0.68
	SON	-0.09	0.28	0.56

- (2) Analysis nudging, i.e., the relaxation of the model solution towards the input fields, was disabled in D1 of the SENS run to let the SST change take full effect and permit modifications in atmospheric dynamics across both domains. Preliminary 1-year test simulations using the REF configuration without nudging showed that the differences in

surface meteorological variables between REF and REF_NO_NUDGE were randomly distributed, with no discernible spatial or temporal trends. This led us to the conclusion that disabling nudging does not cause simulation drift over time, provided that meteorological conditions are updated at high frequency (3-hourly) at the lateral boundaries using a high-resolution driving dataset (ERA5, 31 km). While nudging is widely recognized for reducing model biases and improving the representation of local climate extremes (Bowden et al., 2012; Otte et al., 2012), our focus on seasonal averages in this study is expected to allow comparability between the two datasets, despite the use of nudging in REF D1 but not in SENS.

To assess the impact of the SST increase in 2010–2020 (REF) on climate conditions within the model domains relative to the climatological reference period (1981–2010; SENS), we calculated and compared the differences of REF minus SENS for various meteorological variables. To determine whether the distributions of variables from REF and SENS differ significantly, we used the two-sample, two-tailed Kolmogorov-Smirnov significance test for goodness of fit (KS test; Smirnov, 1933). As a nonparametric test, it does not assume normally distributed data and is therefore suitable for meteorological variables with potentially unknown or non-normal distributions. P-values ≤ 0.05 were considered statistically significant. To account for spatial autocorrelation of meteorological variables in spatial comparisons, we applied a False Discovery Rate (FDR) correction (Wilks, 2006), with the Benjamini and Hochberg (1995) method used for testing and adjustment of p-values. The KS test is relatively sensitive to sample size, hence significant differences were sometimes detected in 3-hourly (D2) but not in daily values (D1).

2 Results and discussion

The analysis is carried out at multiple scales, cascading from large-scale dynamics in D1 (atmospheric circulation and moisture transport), mesoscale effects in D2 (flow patterns and surface climate), to the local climatic conditions in the high mountain environment of the Southern Alps. Changes due to SST increases are broadly similar across seasons, but overall, the most prominent response of atmospheric conditions and processes is seen in summer. Thus, the figures in the following sections focus on the summer season, while other seasons are included in the supplement (Figures S2 and S3).

3.1 Large-scale effects

The SST increase in REF (compared to SENS) strengthens the interactions between the ocean surface and the near-surface atmosphere: Enhanced heat exchange leads to warming of the near-surface atmospheric layer, which fuels evaporation (QFX) based on the Clausius-Clapeyron equation predicting air to hold 7 % more moisture per degree warming globally (Held & Soden, 2006). Consequently, there is a widespread and significant increase in both near-surface (2 m above ground) and atmospheric air temperature (T_2 and T , respectively) as well as moisture content (Q_2 and Q , respectively) across D1, with the spatial distribution of changes in T_2 , Q_2 and QFX reflecting those of SST (Figure S2). Analogous to SST, the average warming and atmospheric moisture increase across D1 are most pronounced in autumn ($+0.37^\circ\text{C}$ and $+0.17\text{ g kg}^{-1}$), followed by summer ($+0.27^\circ\text{C}$ and $+0.14\text{ g kg}^{-1}$).

In response to the surface warming, a thermally induced, widespread but not statistically significant decrease in surface pressure and low-level geopotential height is observed across D1 (Figure 2a). Higher levels (~ 500 hPa and above) are characterized by a corresponding increase in geopotential height. The core of the low-pressure anomaly is centred between the islands, possibly due to a northward expansion of the westerlies and enhanced movement of depressions around the South Island through Cook Strait, as evident from the wind and moisture flux fields (see below). In summer and autumn, the reduction in low-level air pressure may also reflect a slight northward shift of the subtropical high due to ocean warming.

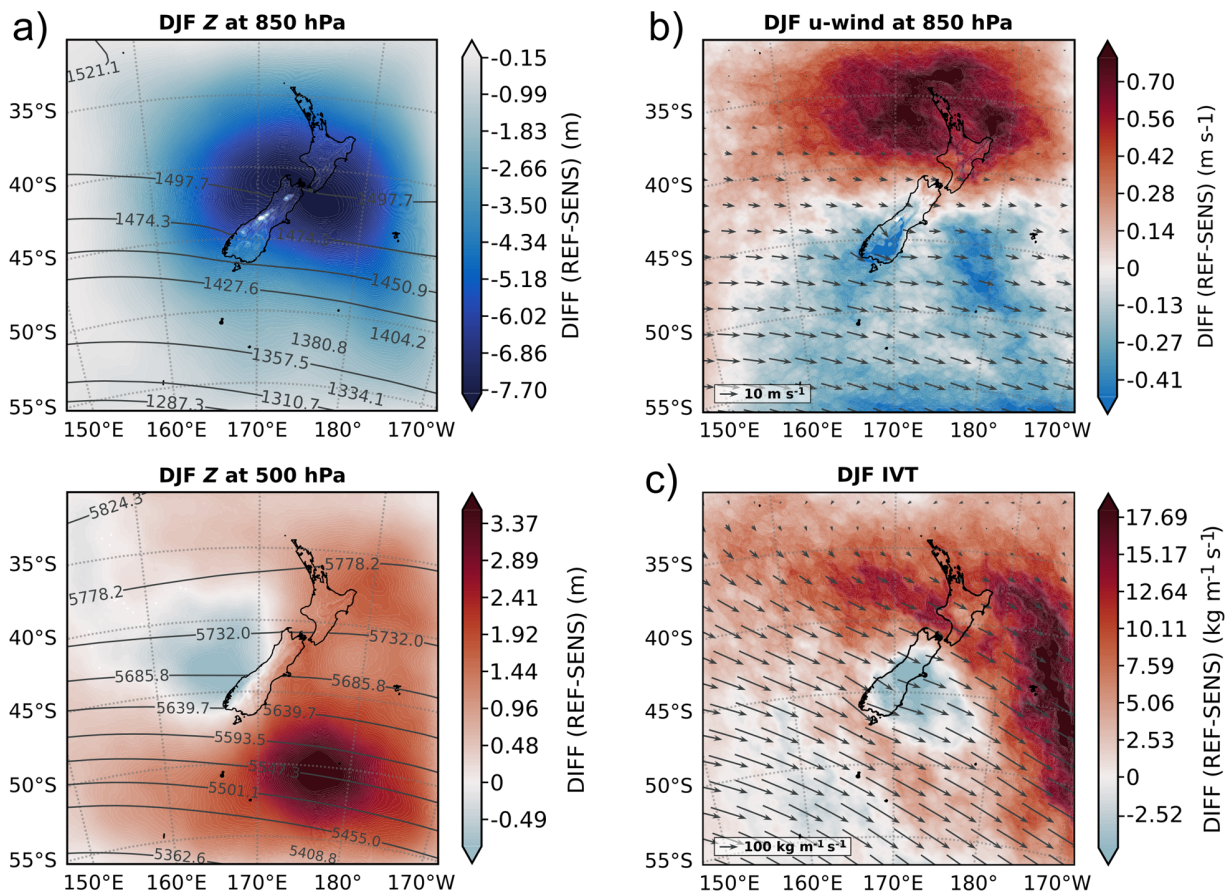


Figure 2. Response of summertime (a) lower and mid-tropospheric geopotential height (Z), (b) low-level u-wind speed, and (c) column integrated water vapor transport (IVT) in D1 to SST increase in 2010–2020. The grey contour lines and arrows indicate the average summertime (a) geopotential height, (b) wind vector, and (c) column integrated moisture flux vector over ocean areas in SENS as an absolute reference. None of the differences is significant (sample size: ~ 1000 times per grid point).

This assumption is further supported by the (insignificant) changes in low-level wind fields, particularly in the zonal u-wind component (Figure 2b). These include (i) a weakening of the easterlies north of 35° S, (ii) a shift towards or strengthening of the westerlies between 35°

S and 43° S, and (iii) a weakening of the westerlies south of 43° S due to a reduced north-south pressure gradient in REF. In winter and spring, when the subtropical high is located further north and westerly winds prevail across the region, there is a strengthening (weakening) of the westerlies north (south) of 40–43° S (Figure S2). The SST-induced changes in pressure and wind patterns contradict future projections of a poleward shift of the Southern Hemisphere subtropical dry zones and mid-latitude storm tracks and jets under climate change (Lee et al., 2021; Seidel et al., 2008), favouring more frequent anticyclonic conditions over New Zealand (Gibson et al., 2016). These differences highlight the importance of this study's focus on the effects of isolated ocean warming rather than coupled changes in the climate system due to global warming. Importantly, insights into the specific role ocean warming plays in modulating regional circulation are assessed in this research.

Column-integrated water vapor transport (IVT) in REF (compared to SENS) shows a weakening over and immediately downstream (east) of the South Island, contrasted by a strengthening of IVT both south and north of the South Island (Figure 2c; not significant). Moisture transport is particularly enhanced along the route from over the north-eastern Tasman Sea through Cook Strait and around the north of the North Island towards the east of New Zealand, affecting the entire North Island and the northern regions of the South Island. The observed change in IVT suggests that under ocean warming, atmospheric moisture transport tends to more frequently circumvent the Southern Alps (rather than flowing over them), favouring pathways around the South Island. This potential change in flow regime is investigated in more detail in the next section since it is a mesoscale feature. Seasonally, the described response of IVT, and by implication the flow regime, is most (least) pronounced in spring and summer (autumn and winter), when the westerlies are generally stronger (weaker).

Most of the changes in large-scale dynamics in D1 are not significant, owing to the daily output frequency of the model in the outer domain, which was chosen to minimize computational expense and storage requirements. However, the detected responses are physically plausible, and many of the examined variables show significant changes based on 3-hourly data in D2 (see below).

3.2 Mesoscale effects

The changes in SST and atmospheric state variables in D1 are manifested in the high-resolution inner domain (D2) through regional modifications. A significant, domain-wide increase in both near-surface and atmospheric air temperature and atmospheric moisture content is observed in all seasons under ocean warming. As in D1, the near-surface warming is most pronounced in autumn (~0.42 °C) and least in spring (~0.25 °C) (Figure S3). The moisture increase is considerably stronger in summer and autumn (~0.20 g kg⁻¹) than in winter and spring (~0.12 g kg⁻¹) (Figure S3). As a response to increased atmospheric temperature and moisture, incoming longwave radiation is significantly enhanced throughout D2 following the Stefan-Boltzmann law, with autumn (winter) exhibiting the strongest (weakest) signal (2.59 W m⁻² and 1.45 W m⁻², respectively). Furthermore, the static stability of air masses over ocean areas is significantly decreased, as indicated by the unsaturated moist Brunt Väisälä Frequency (N_m^2 ; Chen & Lin, 2005) (Figure S3).

Based on the increase in background state atmospheric temperature and moisture content and the changes in large-scale atmospheric dynamics (wind and moisture fluxes), we identify distinct modifications in mesoscale atmospheric processes and near-surface climate variability in D2, which are elaborated in the following subsections.

3.2.1 Change in the orographic effect

Changes in large-scale IVT (see above) suggest a slightly more favoured air flow around rather than over the Southern Alps (and thus, the South Island) under ocean warming (REF). This hypothesis is now being tested and substantiated in the high-resolution domain by a more detailed investigation of the flow regime. The presumable flow regime is described by the Froude Number (Fr) as an interplay between wind speed U perpendicular to the mountain, air mass stability N and barrier height h ($Fr = U/Nh$) (Smith, 1980). Values of $Fr < 1$ characterize a “flow around” regime in which the flow is predominantly blocked and laterally deflected while values > 1 indicate a “flow over” regime in which the incident airflow can readily ascend and descend the mountain range by orographic lifting. High wind speeds and/or low static stability of the approaching air mass tend to favour the “flow over” regime, while low wind speeds and/or high static stability usually result in “flow around”.

Due to the weakening of the westerlies south of $\sim 43^\circ$ S when SSTs are increased (REF) (see above), we observe a decrease in tropospheric wind speed across D2 (Figure 3a), along with a decrease in static stability of the approaching air masses (Figure 3b), thus posing counteracting effects for the response of the flow regime. According to IVT patterns (Figures 2c and 3c), the changes in wind speed appear to be more dominant than changes in static stability, resulting in an increased frequency of flow deflection and less frequent “flow over” events. To explore this further, we defined a sample region a few tens of kilometres upstream of the Southern Alps (Figure 1), in which we calculated the unsaturated moist Froude number ($Fr_m = U/N_m h$) for 10 hPa bin averages between the ground and 750 hPa, corresponding to a barrier height of $h = 2500$ m. We then compared (i) the distribution of 3-hourly Fr_m and (ii) the number of “flow over” events ($Fr_m > 1$) in REF and SENS, respectively. The results indicate that (i) the Southern Alps are generally (in both REF and SENS) within the “flow around” regime, as $Fr \ll 1$ most of the time (not shown). This is consistent with the regime classification of different mountain ranges in Schär (2002). Further, we found that (ii) the highest number of “flow over” events occurs in summer and spring and the lowest in autumn (Figure 4), which is most likely due to the westerlies reaching their maximum (minimum) intensity in spring (autumn) and air mass stability being lowest in summer. The number of “flow over” events in REF is consistently lower across all seasons compared to SENS, with the largest reduction in spring, followed by summer, and the smallest in autumn, resulting in a percentage decrease of “flow over” events of 13 % in spring, 7 % in summer, 4 % in winter and only 1% in autumn (Figure 4). Hence, there is physical evidence that weakened westerlies (despite simultaneously reduced air mass stability) during ocean warming (REF) lead to an adjustment of the flow regime towards more frequent flow deflection (at the expense of “flow over”), resulting in reduced IVT over and downstream of the South Island. The effect is most pronounced in summer and spring, corresponding to the months when “flow over” is generally most pronounced and important.

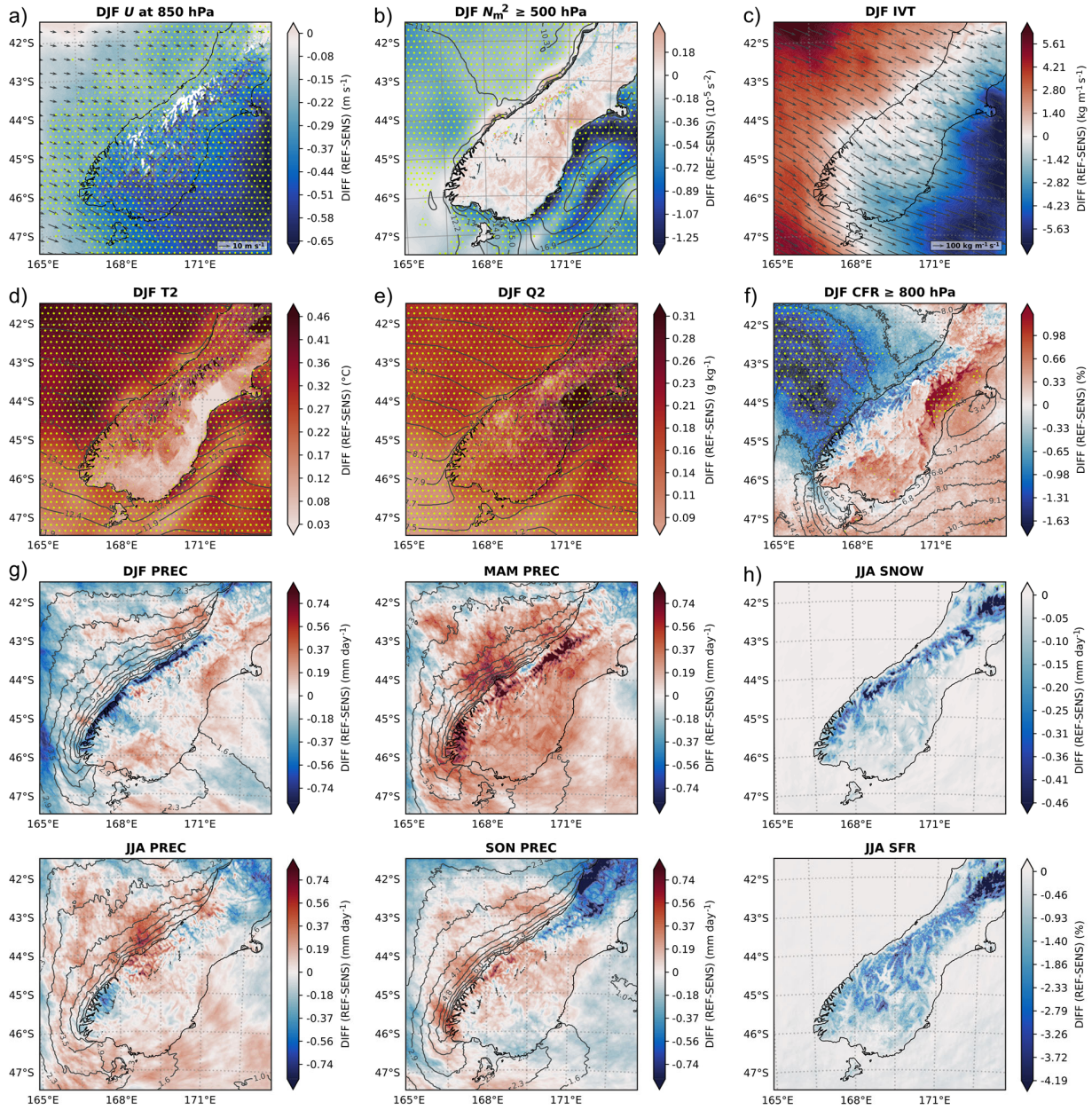


Figure 3. Response of summertime (a) low-level wind speed (U), (b) column-mean (≥ 500 hPa) unsaturated moist Brunt-Väisälä-Frequency (N_m^2), (c) column integrated water vapor transport (IVT), (d) 2m air temperature (T_2), (e) 2m specific humidity (Q_2) and (f) low-level cloud fraction (CFR) in DJF to SST increase in 2010–2020. The same is shown for (g) precipitation (PREC) in all seasons and (h) snowfall (SNOW) and solid fraction of precipitation (SFR) in winter. The grey contour lines and arrows represent the average state of the variables over ocean areas in the respective seasons in SENS as an absolute reference. The yellow dots highlight regions with significant ($p \leq 0.05$) responses.

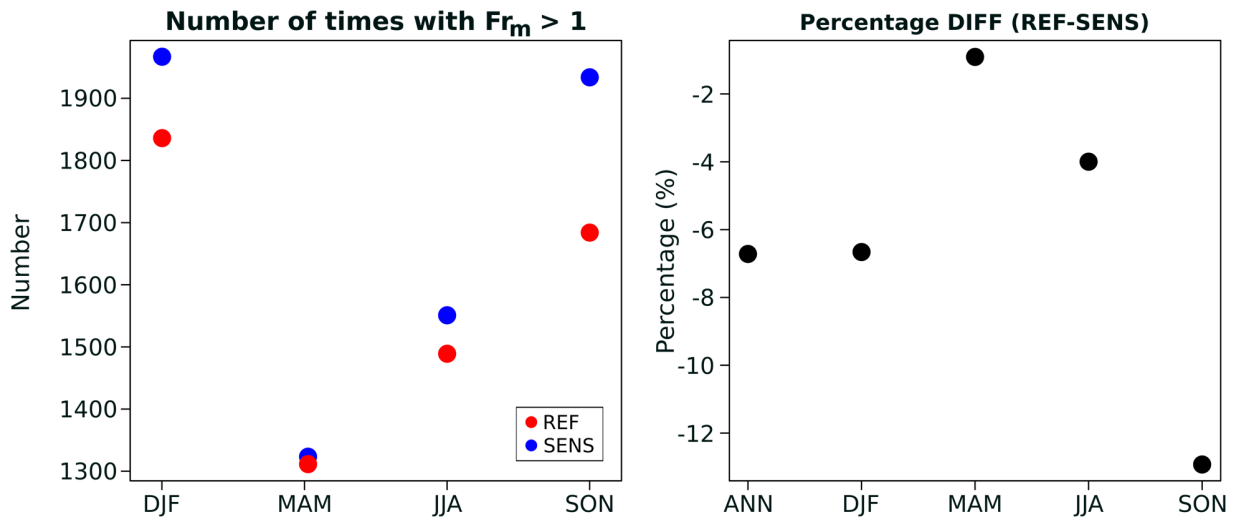


Figure 4. Average number of “flow over” events in REF (ocean warming) and SENS (restricted ocean warming) per season (**left**) and annual and seasonal percentage difference in the number of “flow over” events with respect to SENS (**right**). A “flow over” event was defined as any of the 3-hourly output times and vertical levels (between ground and 750 hPa) having a moist Froude number exceeding one.

On the South Island of New Zealand, “flow over” is typically associated with orographic lifting of the approaching air mass, leading to condensation and large amounts of orographic precipitation on the windward (western) slopes and in the highest-elevation regions of the Southern Alps, while the eastern slopes experience a rain shadow effect and are characterized by warm and dry, relatively strong downslope foehn winds that extend far onto the eastern plains. As these winds predominantly flow across the Southern Alps from a north-westerly direction, they are locally referred to as the nor’wester (Sturman & Tapper, 2006). The rain shadow effect is most pronounced in the South Canterbury region of the Canterbury Plains on the east coast of the South Island, downstream from the highest peaks of the Southern Alps, with the nor’wester being a dominant feature of the local climate in this region (McGowan & Sturman, 1996).

Consistent with a reduced occurrence of “flow over” events with ocean warming (REF), there is evidence of a general, but mainly summertime, weakening of the orographic effect, with less orographic precipitation on the windward side of the mountains and less warming and drying of the near-surface atmosphere by downslope foehn winds in the lee. Air temperature, humidity, cloud fraction, radiation and precipitation show corresponding, distinct responses west and east of the Southern Alps’ Main Divide, especially south of Arthur’s Pass (~43° S):

- The west coast and western slopes are characterized by reduced low-level (≥ 800 hPa) cloud fraction (Figure 3f) and an associated increase in incoming shortwave radiation ($SW\downarrow$) (Figure S3). Incoming longwave radiation ($LW\downarrow$) (Figure S3) is only slightly (but significantly) enhanced, most likely due mainly to the atmosphere’s increased temperature and moisture content, with less influence from cloud feedbacks.

Precipitation decreases along the west coast in summer, when “flow over” is seasonally most important but at the same time shows the strongest decrease in frequency (Figure 3g). The other seasons show a more complex response of precipitation to elevated SSTs, which is discussed in the next section.

- The eastern slopes and east coast show increased low-level cloud fraction and precipitation (Figure 3f-g), along with an increase in incoming longwave radiation and a decrease in shortwave radiation. Q2 is significantly increased (Figure 3e), while T2 displays only a slight, insignificant increase compared to the relatively strong warming observed in the rest of D2 (Figure 3d). The combined effects suggest a less frequent occurrence of the nor’wester in response to ocean warming around New Zealand, resulting in wetter conditions (increased humidity and precipitation) and relatively weak surface warming in the affected regions with respect to the rest of the island. The most affected region, showing the strongest and largely significant response of surface variables, is the foehn-dominated Canterbury Plains.

The observed changes in large-scale circulation (air pressure and winds) and surface climate variability over the South Island induced by increased SSTs around New Zealand are in good agreement with a study by Renwick et al. (1999), who performed 10-year regional model simulations for New Zealand climate for both present-day conditions and for an equilibrium doubling of atmospheric CO₂ concentration, using the Commonwealth Scientific and Industrial Research Organisation (CSIRO) Division of Atmospheric Research (DAR) limited-area model (DARLAM) driven by an atmospheric general circulation model. The CO₂ doubling led to a rise in air temperature and a consequent large-scale decrease in mean sea level pressure and surface westerlies, causing a decrease in east-west gradients in precipitation, temperature and low-level cloud cover. The largest changes were observed over the eastern South Island, in the lee of the highest topography. The authors also noted a decrease in vertical stability and associated enhanced convection. The increase in temperature, as well as the associated weakening of surface winds and the response of precipitation and cloud cover, were most pronounced in winter in this study.

3.2.2 Alteration of precipitation patterns

The response of precipitation to the SST increase in REF is complex. While summer shows a strong decrease in precipitation along the west coast of up to 3.17 mm day⁻¹, and an increase over the eastern lowlands, thereby corroborating the weakening of the orographic effect, other seasons exhibit less clear patterns. In autumn, precipitation increases over both the ocean and the entire South Island, with the largest increase of up to 2.20 mm day⁻¹ occurring in the Southern Alps (Figure 3g). As the westerlies are comparatively weak in autumn – and “flow over” and orographic lifting occurs generally less frequently (see above) – changes in the flow regime are more likely to have a secondary effect on the amount and distribution of precipitation, while thermodynamic processes are likely of greater importance. The observed increase in precipitation may therefore be due to an intensification of convective processes as a result of increased air temperature and humidity (Figure S3). Winter and spring show a mixture of summer and autumn patterns, with some regions experiencing precipitation increases and others decreases (Figure 3g). Examining the underlying physical processes controlling this

regional variability in response is beyond the scope of this study, but we are willing to offer some possible explanations. Spring exhibits a bipolar response, with increased precipitation south of the Mount Cook region and reduced precipitation in the northern part of the Southern Alps. This might be due to a weakening of the westerlies in the north that reduces “flow over”, while the south experiences more moisture availability with only minor changes in flow regime. In winter, precipitation increases mainly occur in the lower-elevation regions around Haast and Arthur’s Pass, which are potentially due to moister air masses preferentially flowing over the Southern Alps in these regions. Higher elevations tend to experience a year-round increase in (mainly liquid) precipitation.

Taking into account D1, where precipitation can be distinguished into stratiform and convective types due to the enabled cumulus parameterization, there is an overall, domain-wide decrease in stratiform precipitation during ocean warming (REF), but an increase in convective precipitation, particularly over the Tasman Sea and along the west coast of the South Island (Figure S2). This is expected due to the enhanced air temperature, humidity and, consequently, instability of air masses (also noted by Renwick et al., 1999), and suggests more forced convection during orographic lifting on the windward side of the Southern Alps. The increase in convective activity is strongest in autumn, when the increase in SST, T2 and Q2 is strongest, consistent with the modelled increase in precipitation in the high-resolution domain.

3.2.3 Decrease in snowfall and solid fraction

Most of the observed changes in total precipitation are due to changes in rainfall patterns. However, in the high-mountain regions and in winter, when snowfall amounts are high, changes in snowfall become crucial for the overall change in precipitation. For glaciers in the Southern Alps, the solid fraction of precipitation, i.e., the proportion that falls as snow, plays a more important role than variations in total precipitation (Anderson et al., 2010) as snowfall directly enhances accumulation and albedo while rainfall promotes melting and ablation and increases glacier velocity (Fitzharris et al., 1999; Porhemmat et al., 2021; Purdie et al., 2008). Typically, the solid-to-liquid ratio is tightly coupled to the freezing point and is therefore most sensitive near the 0 °C isotherm.

We notice a decrease in both snowfall and solid fraction (significant for 3-hourly values, but not significant for daily sums) across the Southern Alps due to the SST increase in REF, which is most pronounced and widespread in winter, with average (local maximum) decreases in snowfall of $-0.04 \text{ mm day}^{-1}$ ($-1.09 \text{ mm day}^{-1}$) and in solid fraction of -0.46% (-7.70%) (Figure 3h). Spring also exhibits high reductions in snowfall, however, mainly within and north of the Mount Cook region ($-0.04 \text{ mm day}^{-1}$ up to $-0.97 \text{ mm day}^{-1}$ and -0.35% up to -5.66% , respectively), while summer and autumn are less strongly affected (Figure S3). Some regions east of the Main Divide show a slight increase in snowfall, especially in autumn and spring, which, however, does not result in positive solid fraction due to concurrently increasing rainfall. The decline in both snowfall and solid fraction is especially strong in the north-eastern Southern Alps beyond Arthur’s Pass, consistent with near-surface warming (see T2 in Figures 3d and S3).

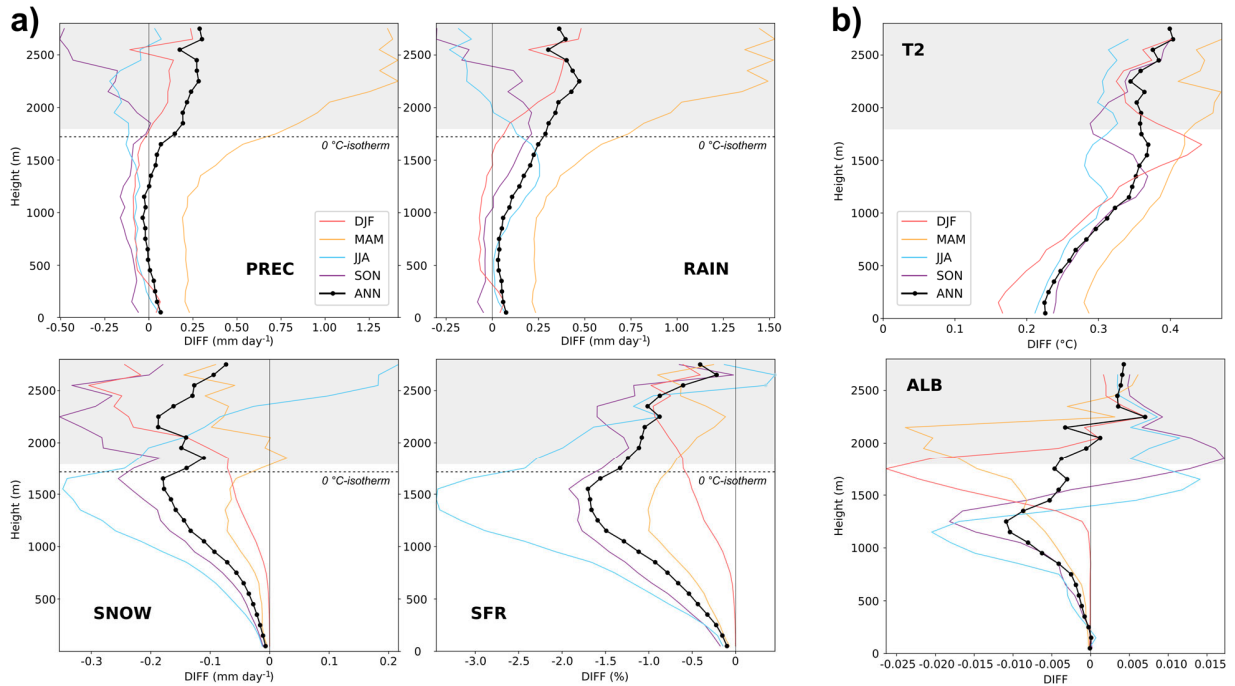


Figure 5. SST-driven annual and seasonal change in (a) precipitation-related variables including total precipitation (PREC), rainfall (RAIN), snowfall (SNOW), and solid fraction (SFR), and (b) 2m air temperature (T2) and albedo (ALB) with respect to altitude. The time series of all terrestrial grid points between the ground and the highest grid cell (~ 2800 m) were averaged within 100 m altitude bins. The grey shaded area highlights the high-elevation environment (≥ 1800 m) used in the local analysis (Sect. 3.2). Significance was not calculated due to the unequal number of grid points within the altitude bins.

The decrease in snowfall tends to increase with altitude (Figure 5a). In winter, the largest reduction (~ 0.35 mm day⁻¹) occurs between 1500 and 1700 m, with less pronounced decreases or even slight increases above 2300 m. Spring and autumn show similar mid-elevation maxima in snowfall reduction (~ 0.25 mm day⁻¹ and ~ 0.07 mm day⁻¹, respectively), but with a further decline at higher elevations. In summer, snowfall decreases consistently with height (up to ~ 0.30 mm day⁻¹). The solid fraction of precipitation reacts similarly to snowfall, but mid elevations show a clearly stronger response than high-elevations, with maximum declines of ~ 3.45 % in winter, ~ 1.92 % in spring and ~ 1.01 % in autumn (Figure 5a). Only summer exhibits a continuous decrease with height (up to ~ 0.98 %). These patterns suggest that reductions in snowfall manifest themselves most strongly in the form of decreasing solid fraction at mid elevations near – specifically, 100–200 m below – the annual mean 0 °C isotherm (1722 m in SENS; dashed line in Figure 5a), where snowfall is most sensitive to warming and most readily converts to rainfall. This is consistent with the understanding that the 0 °C isotherm typically marks the upper boundary of the snow–rain transition zone, an isothermal atmospheric layer of several hundred meters thickness at roughly 0 °C, in which both frozen and liquid hydrometeors coexist (Schauwecker et al., 2022). Notably, solid fraction seems to be related more strongly to the annual mean 0 °C isotherm height than to seasonal

variations (between 1300 m in winter and 2395 m in summer), likely because seasonal mesoscale processes can create a complex solid/liquid transition zone (e.g. Minder et al., 2011), while averaging over the entire year removes such noise and lets the mean background signal appear more clearly. Of interest is that the annual mean 0 °C isotherm is 73 m higher in REF compared to SENS due to the warmer atmospheric conditions, consistent with recent studies that observed an uplift of 0 °C isotherms in response to global warming (Carrasco et al., 2005; Scherrer et al., 2021). This shift is quite remarkable given it is only governed by changes in SST in our dataset. Although the largest declines in solid fraction occur at mid elevations, there are also considerable reductions at higher altitudes, particularly in summer, autumn, and spring.

Height plots such as in Figures 5 and S4 must be interpreted with caution, as potential spatial (west-east and north-south) variations are averaged across all terrestrial grid points per altitude range. When examining the western and eastern slopes of the Southern Alps separately (not shown), the mid-elevation peak in the decrease in snowfall and solid fraction is more pronounced on the western slopes, likely due to most precipitation forming within the orographic cloud on the western side of the Southern Alps. Changes in snowfall and solid fraction are possibly closely related to the mean orographic cloud height. Eastern grid points show a more complex pattern, with a general decrease of snowfall and solid fraction with height (except in winter), probably due to more complex precipitation development. There may also be differing responses in the mountain regions north and south of Arthur's Pass, which we did not investigate in detail.

3.2.4 Elevation-dependent warming

Surface warming in REF increases with altitude, providing evidence of elevation-dependent warming (Figures 3d and 5b). All seasons show a warming peak at mid to high elevations (1100–2200 m), along with a peak decrease in albedo (Figure 5b), with seasonal differences likely related to the varying height of the seasonal snowline. This points to elevation-dependent warming being linked to a positive snow-albedo feedback: warmer air masses lead to enhanced melting and shorter seasonal snow cover, exposing darker, less reflective surfaces (such as firn, ice, or bedrock), which absorb more heat and warm the overlying atmosphere further (Pepin et al., 2015). Snow-albedo feedback processes have been identified as important drivers of elevation-dependent warming in other mountain regions worldwide (Byrne et al., 2024; Chimborazo et al., 2022; Giorgi et al., 1997; Hu & Hsu, 2023; Minder et al., 2018). Unlike changes in snowfall and the snow-to-rain ratio, which are governed more directly by the location of the freezing level, the snowline position is determined by cumulative snowfall during the accumulation season and subsequent melt during the ablation season (Chinn & Chinn, 2020). The highest snowline typically occurs at the end of summer/beginning of autumn (March/April; Willsman & Macara, 2022) due to a lag between peak summer temperatures and the maximum melt rate.

Among seasons, autumn shows the strongest feedback, i.e., the greatest increase in T2 (by 0.47 °C) and decrease in albedo at elevations between 1900 and 2200 m, corresponding to some degree to the mean end-of-summer-snowline (EOSS) for 50 Southern Alps "index" glaciers in 2010–2020 (1925 m; Willsman & Macara, 2022). Summer, spring and winter exhibit

progressively weaker feedbacks with a warming of 0.44 °C, 0.37 °C and 0.31 °C, respectively, at progressively lower elevations of 1600–1800 m, 1200–1400 m and 1100–1200 m.

The summit regions (> 2200 m) are characterized by a further strong increase in T₂, despite a slight increase in albedo. This could be attributed to both increased shortwave radiation and elevated Q₂, the latter leading to enhanced incoming longwave radiation, which raises night-time minimum temperatures. The process is highly sensitive to small changes in Q₂, especially at low levels of Q₂, which generally occur at high altitudes and low temperatures (Pepin et al., 2015; Pepin et al., 2022). Consistent with this, the warming signal in winter and spring is stronger in the highest elevation regions (0.34 °C and 0.40 °C, respectively) than around the snowline.

Warming gradients with altitude are generally higher on the eastern side of the Southern Alps compared to the west, mainly due to weaker warming in the eastern lowlands (not shown). Summer exhibits the strongest increase in T₂ with height, caused by the reduced foehn effect and associated weak warming over the eastern plains. Conversely, the decrease in albedo with altitude is more pronounced on the western side of the Main Divide. Albedo increases observed in winter and spring between 1400 and 2100 m occur mainly on the eastern slopes, potentially due to less frequent foehn winds (Sect. 3.2.1) or an increase in the number of snow-bearing south-easterly events, resulting in greater snow cover during these seasons.

Consequently, increasing SST around New Zealand has led to high elevation regions facing a substantial rise in near-surface air temperatures, thereby providing additional energy for the melting of seasonal snow and glaciers, as well as most likely exerting strong impacts on alpine ecosystems and biota (Chinn & Chinn, 2020). Further ocean warming will likely maintain or exacerbate these effects. The elevation ranges experiencing the strongest warming and largest reductions in albedo coincide with the snowlines and equilibrium line altitudes of glaciers, driving their upward shift, and thus the potential for continued glacier retreat in the Southern Alps. Our findings therefore confirm SST as a contributing factor to the observed trend towards higher regional snowlines since the 1990s, which has intensified since the early 2000s (Lorrey et al., 2022). They also reinforce previous work that has reported positive relationships between SSTs near New Zealand and EOSSs in the Southern Alps (e.g., Clare et al., 2002; Mackintosh et al., 2017), with record high EOSS altitudes observed during marine or coupled ocean-atmosphere heatwaves (Salinger, Renwick, et al., 2019).

3.3 Local-scale effects

While already touched upon, we finally take a more specific look at the impacts of ocean warming on the climatic conditions in the high-elevation regions of the Southern Alps. The zone is defined as all model grid points above 1800 m (299 out of 119716), representing the minimum equilibrium line altitude of New Zealand “index” glaciers in 2010–2020 (Willsman & Macara, 2022). By focusing on these elevations, we aim to infer potential changes in the upper, mainly accumulation-dominated glacier regions that could impact long-term glacier stability. In contrast to the previous sections, in which the average responses to the SST increase over the modelling period (2010–2020) were analysed, this section also examines the development of the signals over time.

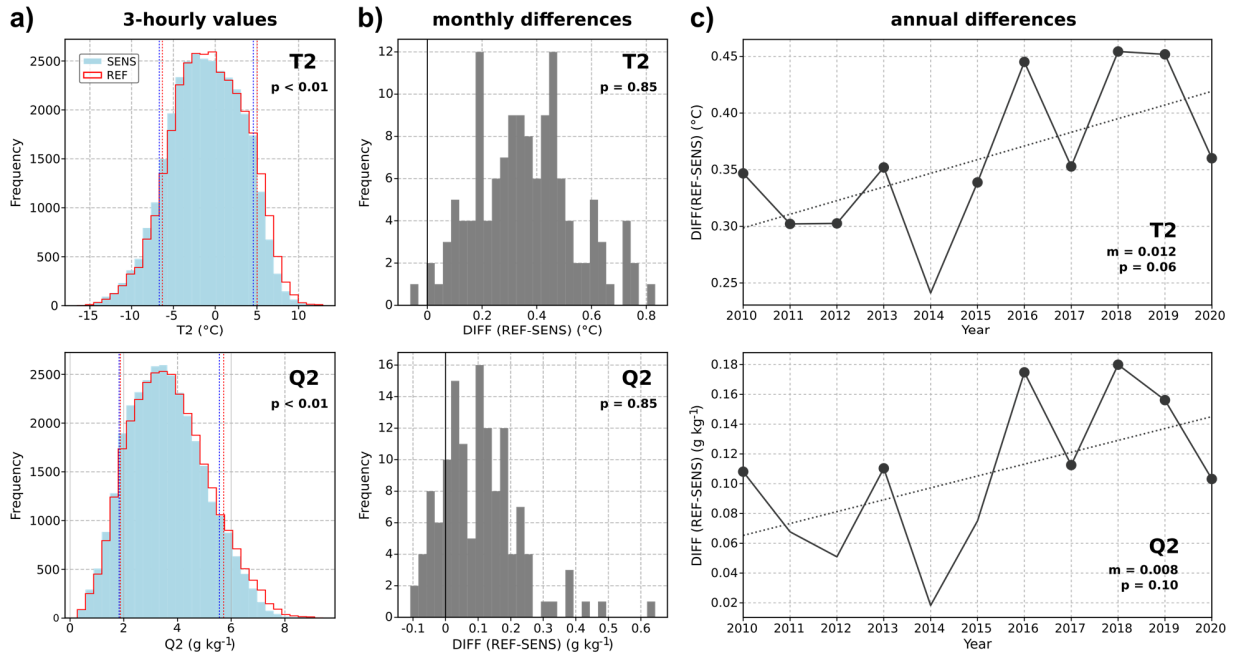


Figure 6. SST-driven change in 2m air temperature (T2; top row) and specific humidity (Q2; bottom row) in the high-mountain environment (≥ 1800 m) in the modelling period (2010–2020): **(a)** frequency distribution of the 3-hourly raw data in REF (ocean warming) and SENS (restricted ocean warming), with dashed vertical lines indicating the 10th and 90th percentile of the respective distribution; **(b)** frequency distribution of monthly mean differences between REF and SENS; **(c)** temporal evolution of annual mean differences over the modelling period, with the dashed gray line indicating the inherent linear trend and filled circles marking years with significant (3-hourly) differences between REF and SENS.

A significant shift in the distribution of 3-hourly and daily near-surface air temperature and specific humidity towards higher values can be observed on average for all high-elevation grid points during ocean warming (REF) (Figure 6), facilitating the occurrence of new extremes. The shift can be observed in all seasons, but is most pronounced in summer and autumn, consistent with the above analyses. The rise in T2 and Q2 is also evident, although not significant, in monthly averages (Figure 6b), with a mean (maximum) monthly warming and moisture increase at high elevations of 0.36 °C (0.83 °C) and 0.11 g kg⁻¹ (0.64 g kg⁻¹), respectively. Considering the temporal development, the differences between REF and SENS exhibit a positive trend for both T2 (+0.01 °C a⁻¹; p = 0.06) and Q2 (+0.01 g kg⁻¹ a⁻¹; p = 0.10) over the modelling period (Figure 6c), indicating that high-altitude regions have experienced progressively warmer and more humid conditions under continued SST increase. The years 2016, 2018 and 2019 stand out with especially high T2 and Q2 increases in REF, suggesting an influence from the prominent marine and coupled ocean-atmosphere heatwaves in these years (Oliver et al., 2017; Salinger et al., 2023).

Other variables show less clear and significant responses to elevated SSTs compared to T2 and Q2. Some, such as precipitation-related variables or incoming shortwave radiation are

naturally right-skewed in their distributions of hourly/daily data, making potential changes or shifts difficult to detect. The overall tendencies of change in various meteorological variables and the associated trend of these changes over the modelling period are summarized in Table 2.

Wind speed shows a clear reduction, particularly in winter and spring, which is significant at 3-hourly and daily resolution. The average (maximum) decline amounts to -0.26 m s^{-1} (-0.85 m s^{-1}) per month, with no discernible trend over time. Incoming radiative fluxes show a tendency towards higher values in REF, also lacking a temporal trend. The increase in incoming longwave radiation is only significant for 3-hourly values and in autumn, with mean (maximum) monthly increases of 1.10 W m^{-2} (11.44 W m^{-2}); incoming shortwave radiation increases by $\sim 1.22 \text{ W m}^{-2}$ per month, with maximum values of 18.88 W m^{-2} per month, however not significantly, regardless of the temporal resolution. The response of albedo is seasonally dependent, with significant shifts to lower values in summer and autumn, but slightly higher values in winter and spring. Over time, summer, autumn and winter tend towards increasingly negative albedo ($p = 0.07$, $p = 0.17$ and $p = 0.04$, respectively), leading to an overall decrease in mean annual albedo throughout the modelling period, especially since 2015, likely driven by the increased frequency of marine and ocean-atmosphere heatwave events.

Table 2. Average response of meteorological surface variables in the high-mountain environment ($\geq 1800 \text{ m}$) to the SST increase in 2010–2020, and temporal trend and significance ($*p \leq 0.1$, $**p \leq 0.05$) of this response based on annual means.

	T2	Q2	U	PSFC	LW↓	SW↓	PREC	RAIN	SNOW	SFR	ALB
Response	↑	↑	↓	↓	↑	↑	↑	↑	↓	↓	↓
11-year trend	↑ **	↑ *	–	↑ **	–	–	–	–	–	–	↑ **

Total precipitation and rainfall show a tendency towards higher amounts in REF, especially since 2015, but changes are small and not statistically significant. The increasing trend over time seems to be driven largely by increasing amounts in autumn that are almost significant ($p = 0.11$ and $p = 0.12$, respectively). Snowfall shows a slight decrease, especially in winter and spring, as well as in annual averages, but significant changes are only evident at the 3-hourly timescale in winter. Similarly, the solid fraction of precipitation is characterized by a general decrease, with statistically significant changes evident on the 3-hourly and daily timescales for the entire period, as well as for 3-hourly values in winter ($p \leq 0.01$), spring ($p = 0.08$), and autumn ($p = 0.03$). There is no significant trend over time for either snowfall or solid fraction.

In summary, we observe changes in high-mountain climate due to gradual increases in SST, which can have serious potential impacts on glaciers and ecosystems. Rising air temperatures in the central and upper regions of glaciers promote the melting of snow and ice and result in more precipitation falling as rain, leaving less snow for accumulation and firn/ice

formation, despite the tendency for total precipitation to increase slightly over time, at least since 2015. In addition, rain-on-snow events have been shown to considerably enhance melting and glacier velocity (Horgan et al., 2015; Kropač et al., 2021; Purdie et al., 2008). These responses will threaten the long-term health of glaciers in the Southern Alps (Rounce et al., 2023) and enhance their demise as ocean warming continues, with implications for regional runoff and freshwater availability.

4 Limitations

While this study generates new insights into how SST affects regional and high-mountain climate in southern New Zealand during gradual climate change through physical processes, some limitations in the experimental design should be noted, which may affect the interpretation of the results.

The use of a LAM for sensitivity experiments introduces certain methodological constraints. LAMs are designed to simulate small-scale processes within a defined domain, relying on externally prescribed lateral boundary conditions, typically sourced from global datasets such as General Circulation Models (GCMs) or reanalyses. For sensitivity experiments involving changes that affect more than just a few grid points, such as large-scale changes in SST, this setup can be challenging because the modifications can alter the internal energy within the regional domain, which can lead to energy accumulating over time, without the possibility for dissipation through the lateral boundaries. This lack of energy exchange with the exterior can result in unrealistic meteorological patterns, particularly in long simulations (Medvigy et al., 2011). Despite this limitation, LAMs have been widely employed in sensitivity experiments (e.g., Collier et al., 2019; Mölg et al., 2012; Noël et al., 2014; Porter et al., 2012; Sierra et al., 2022) as they provide high-resolution, customizable and cost-effective tools (compared to GCMs) for investigating regional atmospheric responses to changes in model physics or lower boundary conditions such as land-use or SST.

Following these previous efforts, we are confident that this approach is suited to investigate the isolated effects of SST variations on New Zealand climate; however, by still being aware of the setup's potential caveats, we have treated the output of the sensitivity run with caution. Importantly, we did not observe any unrealistic patterns or values in key meteorological variables such as temperature or precipitation. For some dynamical variables such as wind and IVT (Figures 2c and S2; mainly the v-components are affected), there is potentially some evidence of accumulating energy (momentum and moisture), especially at the eastern outflow boundary of D1, but the majority of variables are not affected by conspicuous behaviour near the boundaries. Furthermore, the responses observed in the sensitivity run appear physically plausible and explainable, indicating a generally reasonable performance of the model under the modified conditions. Nevertheless, we acknowledge that the sensitivity simulation may not fully capture the magnitude of the SST-induced impacts, as the regional model is constrained by the lack of large-scale energy interactions with the atmosphere outside of D1. The quantitative effects of the SST change are therefore subject to a certain degree of uncertainty.

Another constraint is the use of nudging in REF D1 but not in SENS. Despite preliminary test simulations that showed no evidence of a time drift in the simulations without nudging, we cannot completely rule out that the discrepancy may have introduced other unknown sources of uncertainty, especially for quantitative interpretations. Importantly, the focus on monthly and seasonal time scales in this study means that random differences between REF and SENS at the resolution of single time steps are averaged out, which helps mitigate any uncertainty due to the different use of nudging. Thus, given the lack of evidence of any strong effect imposed by this constraint, we deemed it acceptable (and more sustainable) to not repeat the entire REF simulation.

Lastly, due to the one-way nesting configuration and the treatment of the ocean surface as a quasi-static lower boundary condition in WRF (without including ocean physics), the model simulations do not allow for full domain and ocean–atmosphere interactions. The responses are only unidirectional, with feedbacks from the regional back to the large-scale domain, and feedbacks from the atmosphere back to the ocean, not being accounted for. Since energy fluxes between the ocean and the atmosphere tend to be dampened when feedback processes are considered (Kushnir et al., 2002), the fully coupled atmosphere–ocean system would need to be examined to obtain a more comprehensive understanding of the physical processes at play. Additionally, two-way nesting has been found to improve regional atmospheric simulations (e.g., Madhulatha et al., 2021; Urrego-Blanco et al., 2016), but both approaches demand considerably higher computational expense.

5 Conclusions

This study has investigated the influence of ocean warming on the regional and high-mountain climate of New Zealand, with a particular focus on the high-elevation zones of the Southern Alps, where ecosystems and glaciers are particularly vulnerable to changes in climate. By employing a regional atmospheric model for a sensitivity experiment with modified SST conditions around New Zealand, we demonstrated that the gradual SST increase in 2010–2020 has substantially impacted regional climate dynamics and the near-surface climate in both the lowland regions and, as hypothesized, the high-mountain environment of the Southern Alps, with potential long-term consequences for ecosystems, water resources, and glacier mass balance.

Elevated SSTs were found to cause a large-scale increase in near-surface and atmospheric air temperature and humidity, particularly in autumn and summer, resulting in weakened westerly winds and altered moisture transport pathways, both of which are critical drivers of the weather and climate of New Zealand’s South Island. As a consequence, the mesoscale flow regime of air masses approaching the Southern Alps was modified, reshaping precipitation patterns and reducing the frequency and characteristic impacts of foehn effects in the eastern lowlands of the South Island. The foehn-dominated, typically warm and dry Canterbury Plains were particularly impacted by a transition to wetter conditions and comparatively weak warming. Surface warming generally showed an amplification at higher altitudes, with particularly strong temperature increases near the seasonal snowline, and both snowfall and solid fraction of precipitation experienced notable reductions, especially in winter and around the annual mean 0 °C isotherm. These effects were reflected in a shift in local

climatic conditions in the high alpine environment (≥ 1800 m) of the Southern Alps towards significantly warmer and more humid conditions, contributing to a higher proportion of precipitation falling as rain rather than snow. This has the potential to reduce accumulation while accelerating melt processes, suggesting that ocean warming around New Zealand has contributed to the observed negative mass balance, reduced ice thickness and volume, and retreat of New Zealand glaciers over the last decade (Carrivick et al., 2020; Mackintosh et al., 2017; Vargo et al., 2020). Continued ocean warming in the New Zealand region, as suggested by future projections (Law et al., 2018), is therefore likely to exacerbate glacier retreat, with severe implications for regional hydrology and ecosystems.

Despite some limitations, this study shows clear and physically plausible responses of both the regional and high-altitude climate to increasing SSTs around New Zealand. It should be emphasized that we have only examined the isolated effects of ocean warming, without concurrent changes originating in the atmosphere. Although the results presented here are internally consistent, future climatic changes in the New Zealand region may differ due to broader global climate change dynamics. For instance, GCMs suggest a southward shift of the subtropical high-pressure belt and a strengthening of the westerlies (Lee et al., 2021; Seidel et al., 2008), which could lead to different responses, e.g. in precipitation patterns (Renwick et al., 1999).

Changes in regional and local climate conditions driven by rising SSTs around New Zealand can significantly affect agriculture, tourism, ecosystems, water resources, and communities in New Zealand (Ausseil et al., 2019). Ongoing monitoring and advanced modelling are therefore essential to enhance understanding and develop strategies to address these challenges. Future research could benefit from global and fully coupled ocean-atmosphere models to reduce uncertainties and more accurately quantify impacts of SST changes. The methodology presented here offers the opportunity to investigate relevant topics such as the influence of ocean warming on extreme events or the isolated effects of marine heatwaves.

Conflict of Interest

The authors declare no conflicts of interest relevant to this study.

Acknowledgments

This work was supported by the German Research Foundation (DFG) grants MO 2869/4-1 and MO 2869/4-2. The first author received additional training from the international doctoral program (IDP) “Measuring and Modelling Mountain glaciers and ice caps in a Changing Climate (M³OCCA)”, financed by the Elite Network of Bavaria (ENB) – Bavarian State Ministry of Science and Art. The authors would like to thank Dr. Benjamin Pohl for an insightful discussion on the

limitations of using LAMs in sensitivity experiments. Further, we gratefully acknowledge the scientific support and HPC resources provided by the Erlangen National High Performance Computing Center (NHR@FAU) of the Friedrich-Alexander-Universität Erlangen-Nürnberg (FAU) under the NHR project b128dc / ATMOS ("Numerical atmospheric modelling for the attribution of climate change and for model improvement"). NHR funding is provided by federal and Bavarian state authorities. NHR@FAU hardware is partially funded by the German Research Foundation (DFG) – 440719683.

Data Availability Statement

The Weather Research and Forecasting (WRF) model version 4.2.2 (Skamarock et al., 2019) used to perform the atmospheric simulations is open-source and available from the public WRF-Model Release page on GitHub (<https://github.com/wrf-model/WRF/tree/v4.2.2>). ERA5 reanalysis data (Hersbach et al., 2020) used to drive the model simulations (Hersbach et al., 2023a, 2023b) were downloaded from the Climate Data Store (CDS) via the CDS Application Program Interface (API) (registration required). The reference run of this study is described in detail in Kropač et al. (2024) and is available for download in a condensed form (daily averages, D2 only) at the World Data Center for Climate (WDCC) repository at the German Climate Computation Center (DKRZ) in Hamburg, Germany (Kropač et al., 2023) (CC BY 4.0 licensing; registration required). A more comprehensive version of the reference run as well as data from the sensitivity run are available upon request from the first author (elena.kropac@fau.de). Data analyses and figures were obtained using mainly the following Python packages: wrf-python version 1.3.4.1 (Ladwig, 2017), available from Github (<https://github.com/NCAR/wrf-python>); Matplotlib (Hunter, 2007) version 3.8.3, available from Github (<https://github.com/matplotlib/matplotlib/tree/v3.8.3>); Cartopy version 0.22.0 (Met Office, 2023), available from Github (<https://github.com/SciTools/cartopy/tree/v0.22.0>).

References

- Anderson, B., & Mackintosh, A. (2006). Temperature change is the major driver of late-glacial and Holocene glacier fluctuations in New Zealand. *Geology*, 34(2), 121–124. <https://doi.org/10.1130/G22151.1>
- Anderson, B., Mackintosh, A., Stumm, D., George, L., Kerr, T., Winter-Billington, A., & Fitzsimons, S. (2010). Climate sensitivity of a high-precipitation glacier in New Zealand. *Journal of Glaciology*, 56(195), 114–128. <https://doi.org/10.3189/002214310791190929>
- Ausseil, A. G. E., Daigneault, A. J., Frame, B., & Teixeira, E. I. (2019). Towards an integrated assessment of climate and socio-economic change impacts and implications in New Zealand. *Environmental Modelling & Software*, 119, 1–12. <https://doi.org/10.1016/j.envsoft.2019.05.009>

- 785 Bell, J. J., Micaroni, V., Strano, F., Ryan, K. G., Mitchell, K., Mitchell, P., et al. (2024). Marine
786 heatwave-driven mass mortality and microbial community reorganisation in an
787 ecologically important temperate sponge. *Global Change Biology*, 30(8), e17417.
788 <https://doi.org/10.1111/gcb.17417>
- 789 Benjamini, Y., & Hochberg, Y. (1995). Controlling the false discovery rate: a practical and
790 powerful approach to multiple testing, *Journal of the Royal Statistical Society: Series B*
791 *(Methodological)*, 57(1), 289–300. <https://doi.org/10.1111/j.2517-6161.1995.tb02031.x>
- 792 Bowden, J. H., Otte, T. L., Nolte, C.G., & Otte, M. J. (2012). Examining interior grid nudging
793 techniques using two-way nesting in the WRF Model for regional climate modeling.
794 *Journal of Climate*, 25(8), 2805–2823. <https://doi.org/10.1175/JCLI-D-11-00167.1>
- 795 Bulgin, C. E., Merchant, C. J., & Ferreira, D. (2020). Tendencies, variability and persistence of sea
796 surface temperature anomalies. *Scientific Reports*, 10, 7986.
797 <https://doi.org/10.1038/s41598-020-64785-9>
- 798 Byrne, M. P., Boos, W. R., & Hu, S. (2024). Elevation-dependent warming: observations, models,
799 and energetic mechanisms. *Weather and Climate Dynamics*, 5(2), 763–777.
800 <https://doi.org/10.5194/wcd-5-763-2024>
- 801 Carrasco, J. F., Casassa, G., & Quintana, J. (2005). Changes of the 0°C isotherm and the
802 equilibrium line altitude in central Chile during the last quarter of the 20th century.
803 *Hydrological Sciences Journal*, 50(6), 948. <https://doi.org/10.1623/hysj.2005.50.6.933>
- 804 Carrivick, J. L., James, W. H. M., Grimes, M., Sutherland, J. L., & Lorrey, A. M. (2020). Ice
805 thickness and volume changes across the Southern Alps, New Zealand, from the little ice
806 age to present. *Scientific Reports*, 10, 13392. [https://doi.org/10.1038/s41598-020-](https://doi.org/10.1038/s41598-020-70276-8)
807 [70276-8](https://doi.org/10.1038/s41598-020-70276-8)
- 808 Chen, S.-H., & Lin, Y.-L. (2005). Effects of moist Froude number and CAPE on a conditionally
809 unstable flow over a mesoscale mountain ridge. *Journal of the Atmospheric Sciences*,
810 62(2), 331–350. <https://doi.org/10.1175/JAS-3380.1>
- 811 Chimborazo, O., Minder, J. R., & Vuille, M. (2022). Observations and Simulated Mechanisms of
812 Elevation-Dependent Warming over the Tropical Andes, *Journal of Climate*, 35(3), 1021–
813 1044. <https://doi.org/10.1175/JCLI-D-21-0379.1>
- 814 Chinn, W. G. H., & Chinn, T. J. H. (2020). Tracking the snow line: Responses to climate change by
815 New Zealand alpine invertebrates. *Arctic, Antarctic, and Alpine Research*, 52(1), 361–
816 389. <https://doi.org/10.1080/15230430.2020.1773033>
- 817 Christian, J. E., Siler, N., Koutnik, M., & Roe, G. (2016). Identifying dynamically induced
818 variability in glacier mass-balance records. *Journal of Climate*, 29(24), 8915–8929.
819 <https://doi.org/10.1175/JCLI-D-16-0128.1>
- 820 Clare, G. R., Fitzharris, B. B., Chinn, T. J. H., & Salinger, M. J. (2002). Interannual variation in end-
821 of-summer snowlines of the Southern Alps of New Zealand, and relationships with
822 Southern Hemisphere atmospheric circulation and sea surface temperature patterns.
823 *International Journal of Climatology*, 22(1), 107–120. <https://doi.org/10.1002/joc.722>

- Collier, E., Sauter, T., Mölg, T., & Hardy, D. (2019). The influence of tropical cyclones on circulation, moisture transport, and snow accumulation at Kilimanjaro during the 2006–2007 season. *Journal of Geophysical Research: Atmospheres*, 124(13), 6919–6928. <https://doi.org/10.1029/2019JD030682>
- Cook, F., Smith, R. O., Roughan, M., Cullen, N. J., Shears, N., & Bowen, M. (2022). Marine heatwaves in shallow coastal ecosystems are coupled with the atmosphere: Insights from half a century of daily in situ temperature records. *Frontiers in Climate*, 4, 1012022. <https://doi.org/10.3389/fclim.2022.1012022>
- Cullen, N. J., Gibson, P. B., Mölg, T., Conway, J. P., Sirguey, P., & Kingston, D. G. (2019). The influence of weather systems in controlling mass balance in the Southern Alps of New Zealand. *Journal of Geophysical Research: Atmospheres*, 124(8), 4514–4529. <https://doi.org/10.1029/2018JD030052>
- Fitzharris, B. B., Clare, G. R., & Renwick, J. (2007). Teleconnections between Andean and New Zealand glaciers. *Global and Planetary Change*, 59(1–4), 159–174. <https://doi.org/10.1016/j.gloplacha.2006.11.022>
- Fitzharris, B., Lawson, W., & Owens, I. (1999). Research on glaciers and snow in New Zealand. *Progress in Physical Geography: Earth and Environment*, 23(4), 469–500. <https://doi.org/10.1177/030913339902300402>
- Gibson, P. B., Perkins-Kirkpatrick, S. E., & Renwick, J. A. (2016). Projected changes in synoptic weather patterns over New Zealand examined through self-organizing maps. *International Journal of Climatology*, 36(12), 3934–3948. <https://doi.org/10.1002/joc.4604>
- Giorgi, F., Hurrell, J. W., Marinucci, M. R., & Beniston, M. (1997). Elevation dependency of the surface climate change signal: A model study. *Journal of Climate*, 10(2), 288–296. [https://doi.org/10.1175/1520-0442\(1997\)010<0288:EDOTSC>2.0.CO;2](https://doi.org/10.1175/1520-0442(1997)010<0288:EDOTSC>2.0.CO;2)
- Griffiths, G. A., & McSaveney, M. J. (1983). Distribution of mean annual precipitation across some steepland regions of New Zealand. *New Zealand Journal of Science*, 26, 197–209.
- Held, I. M., & Soden, B. J. (2006). Robust responses of the hydrological cycle to global warming. *Journal of Climate*, 19(21), 5686–5699. <https://doi.org/10.1175/JCLI3990.1>
- Hersbach, H., Bell, B., Berrisford, P., Biavati, G., Horányi, A., Muñoz Sabater, J., et al. (2023a). ERA5 hourly data on single levels from 1940 to present [Dataset]. Copernicus Climate Change Service (C3S) Climate Data Store (CDS). <https://doi.org/10.24381/cds.adbb2d47>
- Hersbach, H., Bell, B., Berrisford, P., Biavati, G., Horányi, A., Muñoz Sabater, J., et al. (2023b). ERA5 hourly data on pressure levels from 1940 to present [Dataset]. Copernicus Climate Change Service (C3S) Climate Data Store (CDS). <https://doi.org/10.24381/cds.bd0915c6>
- Hersbach, H., Bell, B., Berrisford, P., Hirahara, S., Horányi, A., Muñoz-Sabater, J., et al. (2020). The ERA5 global reanalysis. *Quarterly Journal of the Royal Meteorological Society*, 146(730), 1999–2049. <https://doi.org/10.1002/qj.3803>

- Hobday, A. J., & Pecl, G. T. (2014). Identification of global marine hotspots: sentinels for change and vanguards for adaptation action. *Reviews in Fish Biology and Fisheries*, 24, 415–425. <https://doi.org/10.1007/s11160-013-9326-6>
- Horgan, H. J., Anderson, B., Alley, R. B., Chamberlain, C., J., Dykes, R., Kehrl, L. M., & Townend, J. (2015). Glacier velocity variability due to rain-induced sliding and cavity formation. *Earth and Planetary Science Letters*, 432, 273–282. <https://doi.org/10.1016/j.epsl.2015.10.016>
- Hu, S., & Hsu, P.-C. (2023). Drivers of elevation-dependent warming over the Tibetan Plateau. *Atmospheric and Oceanic Science Letters*, 16(2), 100289. <https://doi.org/10.1016/j.aosl.2022.100289>
- Hunter, J. D. (2007). Matplotlib: A 2D Graphics Environment. *Computing in Science & Engineering*, 9(3), 90–95. <https://doi.org/10.1109/MCSE.2007.55>
- Jung, S.-H., Im, E.-S., & Han, S.-O. (2012). The effect of topography and sea surface temperature on heavy snowfall in the Yeongdong region: A case study with high resolution WRF simulation. *Asia-Pacific Journal of Atmospheric Sciences*, 48, 259–273. <https://doi.org/10.1007/s13143-012-0026-2>
- Keegan, L. J., White, R. S. A., & Macinnis-Ng, C. (2022). Current knowledge and potential impacts of climate change on New Zealand’s biological heritage. *New Zealand Journal of Ecology*, 46(1), 3467. doi:10.20417/nzjecol.46.10
- Kittel, C., Amory, C., Agosta, C., Delhasse, A., Doutreloup, S., Huot, P.-V., et al. (2018). Sensitivity of the current Antarctic surface mass balance to sea surface conditions using MAR. *The Cryosphere*, 12(12), 3827–3839. <https://doi.org/10.5194/tc-12-3827-2018>
- Kropač, E., Mölg, T., & Cullen, N. J. (2023). 16-year WRF simulation for the Southern Alps of New Zealand [Dataset]. World Data Center for Climate (WDCC) at DKRZ. https://doi.org/10.26050/WDCC/NZ-PROXY_16yrWRF
- Kropač, E., Mölg, T., & Cullen, N. J. (2024). A new, high-resolution atmospheric dataset for southern New Zealand, 2005–2020, *Geoscience Data Journal*, 11(4), 873–895, <https://doi.org/10.1002/gdj3.263>
- Kropač, E., Mölg, T., Cullen, N. J., Collier, E., Pickler, C., & Turton, J. V. (2021). A detailed, multi-scale assessment of an atmospheric river event and its impact on extreme glacier melt in the Southern Alps of New Zealand. *Journal of Geophysical Research: Atmospheres*, 126(9), e2020JD034217. <https://doi.org/10.1029/2020JD034217>
- Kushnir, Y., Robinson, W. A., Bladé, I., Hall, N. M. J., Peng, S., & Sutton, R. (2002). Atmospheric GCM Response to Extratropical SST Anomalies: Synthesis and Evaluation, *Journal of Climate*, 15(16), 2233–2256, [https://doi.org/10.1175/1520-0442\(2002\)015<2233:AGRTES>2.0.CO;2](https://doi.org/10.1175/1520-0442(2002)015<2233:AGRTES>2.0.CO;2)
- Ladwig, W. (2017). wrf-python (Version 3.4.1) [Software]. Boulder, CO, USA: UCAR/NCAR. <https://doi.org/10.5065/D6W094P1>
- Lavender, S. L., Hoeke, R. K., & Abbs, D. J. (2018). The influence of sea surface temperature on the intensity and associated storm surge of tropical cyclone Yasi: a sensitivity study,

- Natural Hazards and Earth System Sciences*, 18(3), 795–805,
<https://doi.org/10.5194/nhess-18-795-2018>
- Law, C. S., Rickard, G. J., Mikaloff-Fletcher, S. E., Pinkerton, M. H., Behrens, E., Chiswell, S. M., & Currie, K. (2018). Climate change projections for the surface ocean around New Zealand, *New Zealand Journal of Marine and Freshwater Research*, 52(3), 309–335,
<https://doi.org/10.1080/00288330.2017.1390772>
- Lee, J.-Y., Marotzke, J., Bala, G., Cao, L., Corti, S., Dunne, J. P., et al. (2021). Future Global Climate: Scenario-Based Projections and Near-Term Information. In V. Masson-Delmotte et al. (Eds.), *Climate Change 2021: The Physical Science Basis. Contribution of Working Group I to the Sixth Assessment Report of the Intergovernmental Panel on Climate Change* (pp. 553–672). Cambridge, UK and New York, NY, USA: Cambridge University Press.
- Lorrey, A. M., Vargo, L., Purdie, H., Anderson, B., Cullen, N. J., Sirguey, P., et al. (2022). Southern Alps equilibrium line altitudes: four decades of observations show coherent glacier–climate responses and a rising snowline trend, *Journal of Glaciology*, 68(272), 1127–1140. <https://doi.org/10.1017/jog.2022.27>
- Mackintosh, A. N., Anderson, B. M., Lorrey, A. M., Renwick, J. A., Frei, P., & Dean, S. M. (2017). Regional cooling caused recent New Zealand glacier advances in a period of global warming, *Nature Communications*, 8, 14202, <https://doi.org/10.1038/ncomms14202>
- Madhulatha, A., Choi, S. J., Han, J. Y., & Hong, S. Y. (2021). Impact of different nesting methods on the simulation of a severe convective event over South Korea using the Weather Research and Forecasting Model, *Journal of Geophysical Research: Atmospheres*, 126(5), e2020JD033084, <https://doi.org/10.1029/2020JD033084>
- McGowan, H. A., & Sturman, A. P. (1996). Regional and local scale characteristics of foehn wind events over the South Island of New Zealand, *Meteorology and Atmospheric Physics*, 58, 151–164, <https://doi.org/10.1007/BF01027562>
- Medvigy, D., Walko, R. L., & Avissar, R. (2011). Effects of deforestation on spatiotemporal distributions of precipitation in south America, *Journal of Climate*, 24(8), 2147–2163, <https://doi.org/10.1175/2010JCLI3882.1>
- Met Office (2023). Cartopy: a cartographic python library with a Matplotlib interface (Version 0.22.0) [Software]. Exeter, Devon, UK: Met Office.
<https://github.com/SciTools/cartopy/tree/v0.22.0>
- Miglietta, M. M., Moscatello, A., Conte, D., Mannarini, G., Lacorata, G., & Rotunno, R. (2011). Numerical analysis of a Mediterranean ‘hurricane’ over south-eastern Italy: Sensitivity experiments to sea surface temperature. *Atmospheric Research*, 101(1–2), 412–426.
<https://doi.org/10.1016/j.atmosres.2011.04.006>
- Minder, J. R., Durran, D. R., & Roe, G. H. (2011). Mesoscale controls on the mountainside snow line. *Journal of the Atmospheric Sciences*, 68(9), 2107–2127.
<https://doi.org/10.1175/JAS-D-10-05006.1>

- Minder, J. R., Letcher, T. W., & Liu, C. (2018). The character and causes of elevation-dependent warming in high-resolution simulations of Rocky Mountain climate change. *Journal of Climate*, 31(6), 2093–2113. <https://doi.org/10.1175/JCLI-D-17-0321.1>
- Mölg, T., Großhauser, M., Hemp, A., Hofer, M., & Marzeion, B. (2012). Limited forcing of glacier loss through land-cover change on Kilimanjaro. *Nature Climate Change*, 2, 254–258. <https://doi.org/10.1038/nclimate1390>
- Montie, S., Thorat, F., Smith, R. O., Cook, F., Tait, L. W., Pinkerton, M. H., et al. (2024). Seasonal trends in marine heatwaves highlight vulnerable coastal ecoregions and historic change points in New Zealand. *New Zealand Journal of Marine and Freshwater Research*, 58(2), 274–299. <https://doi.org/10.1080/00288330.2023.2218102>
- Noël, B., Fettweis, X., van de Berg, W. J., van den Broeke, M. R., & Erpicum, M. (2014). Sensitivity of Greenland Ice Sheet surface mass balance to perturbations in sea surface temperature and sea ice cover: a study with the regional climate model MAR. *The Cryosphere*, 8(5), 1871–1883. <https://doi.org/10.5194/tc-8-1871-2014>
- Oliver, E. C. J. (2019). Mean warming not variability drives marine heatwave trends. *Climate Dynamics*, 53, 1653–1659. <https://doi.org/10.1007/s00382-019-04707-2>
- Oliver, E. C. J., Benthuyssen, J. A., Bindoff, N. L., Hobday, A. J., Holbrook, N. J., Mundy, C. N., & Perkins-Kirkpatrick, S. E. (2017). The unprecedented 2015/16 Tasman Sea marine heatwave. *Nature Communications*, 8, 16101. <https://doi.org/10.1038/ncomms16101>
- Otte, T. L., Nolte, C. G., Otte, M. J., & Bowden, J. H. (2012). Does Nudging Squelch the Extremes in Regional climate modeling? *Journal of Climate*, 25(20), 7046–7066. <https://doi.org/10.1175/JCLID-12-00048.1>
- Pepin, N. C., Arnone, E., Gobiet, A., Haslinger, K., Kotlarski, S., Notarnicola, C., et al. (2022). Climate changes and their elevational patterns in the mountains of the world. *Reviews of Geophysics*, 60(1), e2020RG000730. <https://doi.org/10.1029/2020RG000730>
- Pepin, N. C., Bradley, R. S., Diaz, H. F., Baraer, M., Caceres, E. B., Forsythe, N., et al. (2015). Elevation-dependent warming in mountain regions of the world. *Nature Climate Change*, 5, 424–430. <https://doi.org/10.1038/nclimate2563>
- Porhemmat, R., Purdie, H., Zawar-Reza, P., Zammit, C., & Kerr, T. (2021). Moisture transport during large snowfall events in the New Zealand Southern Alps: the role of atmospheric rivers. *Journal of Hydrometeorology*, 22(2), 425–444. <https://doi.org/10.1175/JHM-D-20-0044.1>
- Porter, D. F., Cassano, J. J., & Serreze, M. C. (2012). Local and large-scale atmospheric responses to reduced Arctic Sea ice and ocean warming in the WRF model. *Journal of Geophysical Research: Atmospheres*, 117(D11), D11115. <https://doi.org/10.1029/2011JD016969>
- Powers, J. G., Klemp, J. B., Skamarock, W. C., Davis, C. A., Dudhia, J., Gill, D. O., et al. (2017). The weather research and forecasting model: Overview, system efforts, and future directions. *Bulletin of the American Meteorological Society*, 98(8), 1717–1737. <https://doi.org/10.1175/bams-d-15-00308.1>

- 979 Purdie, H. L., Brook, M. S., & Fuller, I. C. (2008). Seasonal variation in ablation and surface
980 velocity on a temperate maritime glacier: Fox Glacier, New Zealand. *Arctic, Antarctic,
981 and Alpine Research*, 40(1), 140–147. [https://doi.org/10.1657/1523-0430\(06-
982 032\)\[PURDIE\]2.0.CO;2](https://doi.org/10.1657/1523-0430(06-032)[PURDIE]2.0.CO;2)
- 983 Purdie, H., Mackintosh, A., Lawson, W., Anderson, B., Morgenstern, U., Chinn, T., & Mayewski,
984 P. (2011). Interannual variability in net accumulation on Tasman Glacier and its
985 relationship with climate. *Global and Planetary Change*, 77(3–4), 142–152.
986 <https://doi.org/10.1016/j.gloplacha.2011.04.004>
- 987 Renwick, J. A., Katzfey, J. J., McGregor, J. L., & Nguyen, K. C. (1999). On regional model
988 simulations of climate change over New Zealand. *Weather and Climate*, 19, 3–13.
989 <https://doi.org/10.2307/44279923>
- 990 Rounce, D. R., Hock, R., Maussion, F., Hugonnet, R., Kochtitzky, W., Huss, M., et al. (2023).
991 Global glacier change in the 21st century: Every increase in temperature matters.
992 *Science*, 379(6627), 78–83. <https://doi.org/10.1126/science.abo1324>
- 993 Salinger, M. J., Diamond, H. J., Bell, J., Behrens, E., Fitzharris, B. B., Herod, N., et al. (2023).
994 Coupled ocean-atmosphere summer heatwaves in the New Zealand region: an update.
995 *Weather and Climate*, 42(1), 18–41. <https://doi.org/10.2307/27226713>
- 996 Salinger, M. J., Fitzharris, B. B., & Chinn, T. (2019). Atmospheric circulation and ice volume
997 changes for the small and medium glaciers of New Zealand's Southern Alps mountain
998 range 1977–2018. *International Journal of Climatology*, 39(11), 4274–4287.
999 <https://doi.org/10.1002/joc.6072>
- 1000 Salinger, M. J., Renwick, J., Behrens, E., Mullan, A. B., Diamond, H. J., Sirguey, P., et al. (2019).
1001 The unprecedented coupled ocean-atmosphere summer heatwave in the New Zealand
1002 region 2017/18: drivers, mechanisms and impacts. *Environmental Research Letters*,
1003 14(4), 044023. <https://doi.org/10.1088/1748-9326/ab012a>
- 1004 Schär, C. (2002). Mesoscale mountains and the larger-scale atmospheric dynamics: A review.
1005 *International Geophysics*, 83, 29–42. [https://doi.org/10.1016/S0074-6142\(02\)80155-3](https://doi.org/10.1016/S0074-6142(02)80155-3)
- 1006 Schauwecker, S., Palma, G., MacDonell, S., Ayala, Á., & Viale, M. (2022). The Snowline and 0°C
1007 Isotherm Altitudes During Precipitation Events in the Dry Subtropical Chilean Andes as
1008 Seen by Citizen Science, Surface Stations, and ERA5 Reanalysis Data. *Frontiers in Earth
1009 Science*, 10, 875795. <https://doi.org/10.3389/feart.2022.875795>
- 1010 Scherrer, S. C., Gubler, S., Wehrli, K., Fischer, A. M., & Kotlarski, S. (2021). The Swiss Alpine zero
1011 degree line: Methods, past evolution and sensitivities. *International Journal of
1012 Climatology*, 41(15), 6785–6804. <https://doi.org/10.1002/joc.v41.1510.1002/joc.7228>
- 1013 Seidel, D., Fu, Q., Randel, W., & Reichler, T. J. (2008). Widening of the tropical belt in a changing
1014 climate. *Nature Geoscience*, 1, 21–24. <https://doi.org/10.1038/ngeo.2007.38>
- 1015 Shears, N. T., & Bowen, M. M. (2017). Half a century of coastal temperature records reveal
1016 complex warming trends in western boundary currents. *Scientific Reports*, 7, 14527.
1017 <https://doi.org/10.1038/s41598-017-14944-2>

- 1018 Shears, N. T., Bowen, M. M., & Thorat, F. (2024). Long-term warming and record-breaking
1019 marine heatwaves in the Hauraki Gulf, northern New Zealand. *New Zealand Journal of*
1020 *Marine and Freshwater Research*, 1–12.
1021 <https://doi.org/10.1080/00288330.2024.2319100>
- 1022 Sierra, J. P., Junquas, C., Espinoza, J. C., Segura, H., Condom, T., Andrade, M., et al. (2022).
1023 Deforestation impacts on Amazon-Andes hydroclimatic connectivity. *Climate Dynamics*,
1024 58, 2609–2636. <https://doi.org/10.1007/s00382-021-06025-y>
- 1025 Sijikumar, S., & Rajeev, K. (2012). Role of the Arabian Sea warm pool on the precipitation
1026 characteristics during the monsoon onset period. *Journal of Climate*, 25(6), 1890–1899.
1027 <https://doi.org/10.1175/JCLI-D-11-00286.1>
- 1028 Skamarock, W. C., Klemp, J. B., Dudhia, J., Gill, D. O., Liu, Z., Berner, J., et al. (2019). A
1029 Description of the Advanced Research WRF Model Version 4. In *NCAR Technical Notes*
1030 (NCAR/TN-915 556+STR, pp. 1–145). Boulder, CO, USA: National Center for Atmospheric
1031 Research.
- 1032 Smirnov, N. V. (1933). Estimate of deviation between empirical distribution functions in two
1033 independent samples. *Bulletin Moscow University*, 2, 3–16.
- 1034 Smith, R. B. (1980). Linear theory of stratified hydrostatic flow past an isolated mountain.
1035 *Tellus*, 32(4), 348–364. <https://doi.org/10.1111/j.2153-3490.1980.tb00962.x>
- 1036 Stauffer, D. R., & Seaman, N. L. (1994). Multiscale Four-Dimensional Data Assimilation. *Journal*
1037 *of Applied Meteorology and Climatology*, 33(3), 416–434. [https://doi.org/10.1175/1520-](https://doi.org/10.1175/1520-0450(1994)033<0416:MFDDA>2.0.CO;2)
1038 [0450\(1994\)033<0416:MFDDA>2.0.CO;2](https://doi.org/10.1175/1520-0450(1994)033<0416:MFDDA>2.0.CO;2)
- 1039 Steiger, R., Knowles, N., Pöll, K., & Rütty, M. (2024). Impacts of climate change on mountain
1040 tourism: a review. *Journal of Sustainable Tourism*, 32(9), 1984–2017.
1041 <https://doi.org/10.1080/09669582.2022.2112204>
- 1042 Sturman, A. P., & Tapper, N. J. (Eds.) (2006). *The Weather and Climate of Australia and New*
1043 *Zealand* (2nd ed.). Melbourne, Australia: Oxford University Press.
- 1044 Sutton P. J. H., & Bowen, M. (2019). Ocean temperature change around New Zealand over the
1045 last 36 years. *New Zealand Journal of Marine and Freshwater Research*, 53(3), 305–326.
1046 <https://doi.org/10.1080/00288330.2018.1562945>
- 1047 Takahashi, H. G., Adachi, S. A., Sato, T., Hara, M., Ma, X., & Kimura, F. (2015). An oceanic impact
1048 of the Kuroshio on surface air temperature on the pacific coast of Japan in summer:
1049 Regional H2O greenhouse gas effect. *Journal of Climate*, 28(18), 7128–7144.
1050 <https://doi.org/10.1175/JCLI-D-14-00763.1>
- 1051 Thomsen, M. S., Mondardini, L., Alestra, T., Gerrity, S., Tait, L., South, P. M., et al. (2019). Local
1052 extinction of bull kelp (*Durvillaea* spp.) due to a marine heatwave. *Frontiers in Marine*
1053 *Science*, 6, 84. <https://doi.org/10.3389/fmars.2019.00084>
- 1054 Urrego-Blanco, J. Sheng, J., & Dupont, F. (2016). Performance of one-way and two-way nesting
1055 techniques using the shelf circulation modelling system for the eastern Canadian shelf.
1056 *Atmosphere-Ocean*, 54(1), 75–92. <https://doi.org/10.1080/07055900.2015.1130122>

- Vargo, L. J., Anderson, B. M., Dadić, R., Horgan, H. J., Mackintosh, A. N., King, A. D., & Lorrey, A. M. (2020). Anthropogenic warming forces extreme annual glacier mass loss. *Nature Climate Change*, 10, 856–861. <https://doi.org/10.1038/s41558-020-0849-2>
- Vuille, M., Kaser, G., & Juen, I. (2008). Glacier mass balance variability in the Cordillera Blanca, Peru and its relationship with climate and the large-scale circulation. *Global and Planetary Change*, 62(1–2), 14–28. <https://doi.org/10.1016/j.gloplacha.2007.11.003>
- Wilks, D. S. (2006). On “Field Significance” and the False Discovery Rate. *Journal of Applied Meteorology and Climatology*, 45(9), 1181–1189. <https://doi.org/10.1175/JAM2404.1>
- Willsman, A., & Macara, G. (2022). New Zealand Glacier Monitoring: End of summer snowline survey 2020. In *NIWA Client Reports* (No. 2022014EI, pp. 1–160), Dunedin, New Zealand: National Institute of Water & Atmospheric Research Ltd.